X-ray computed tomography evaluations of additive manufactured multi-material composites.

Journal:	*Journal of Microscopy*
Manuscript ID	JMI-2020-0106
Wiley - Manuscript type:	Themed Issue Paper
Date Submitted by the Author:	22-Jun-2020
Complete List of Authors:	Curto, Marco; University of Portsmouth, School of mechanical and design engineering Kao, Alexander; University of Portsmouth, School of Engineering Tozzi, Gianluca; University of Portsmouth School of Engineering, Barber, Asa; London South Bank University, Engineering
Keywords:	X-ray computed tomography, Additive Manufacturing, 3D printing, Composites, Multi-material

X-ray computed tomography evaluations of additive manufactured multi-material composites

M. Curto*, A. P. Kao*§, G. Tozzi*§, A. H. Barber†

* School of Mechanical and Design Engineering, University of Portsmouth, Portsmouth, UK
§ Zeiss Global Centre, University of Portsmouth, Portsmouth, UK
† School of Engineering, London South Bank University, United Kingdom

Abstract

Additive Manufacturing (AM) often produces complex engineered structures by precisely distributing materials in a layer by layer fashion. Multi-material AM is a particularly flexible technique able to combine a range of hard and soft materials to produce designed composites. Critically, the design of AM multi-material structures requires the development of precise three-dimensional (3D) computer aided design (CAD) files. While such digital design is highly employed, techniques able to validate the physically manufactured composite against the digital design from which it is generated are lacking for AM, especially as any evaluations must be able to distinguish material variation across the 3D space. In this paper, a non-destructive approach using X-ray computed tomography (XCT) is used to fully evaluate the 3D distribution of multi-materials from an AM process. Specifically, two diverse hard and soft materials are alternatively produced in the form of a fibre embedded in a matrix. XCT coupled with imaging evaluation were able to distinguish between the differing materials and, importantly, to demonstrate a reduction in the expected fabricated volumes when compared to the respective CAD designs.

Keywords: X-ray computed tomography, Additive Manufacturing, 3D printing, Composites, Multi-material.

* Corresponding author. Tel.: + 44 7546 620604
Email address: marco.curto@port.ac.uk (Marco Curto)

Introduction

Three-dimensional (3D) additive layer manufacturing (AM), commonly referred to as 3D printing, has shown significant potential in fabricating complex parts. The attractiveness of AM is based on digital designs, with almost arbitrary shape and complexity being translated to a physical model through additive material deposition[1]. Limits in free form fabrication of classical manufacturing such as mould jetting and CNC machining have been overcome using AM approaches[2 3 4 5]. The flexibility of AM lies in the development of computed aided design (CAD) that are subsequently translated in standard tessellation language (STL), which controls the physical production of either simple mono-material or more organised multi-material parts. For the latter, multi-material AM has attracted the attention of material scientists due to its ability to construct engineered composites. The recent availability of multi-jetting technology is of significant importance and, as a result of this importance, has led to the recognition within ISO and ASTM international standards[6 7 8]. However, techniques able to validate the digital designs of the AM composite with the ability to evaluate compositional changes across the 3D space are lacking. Common inspection methods, such as optical microscopy (OM) and scanning electron microscopy (SEM), are widely used to provide detailed topological and compositional information inspecting the surface of a sample before or after testing. Compositional information can be further provided integrating SEM with an energy Dispersive X-ray spectrometry systems (EDS)[9] but both SEM and EDS fundamentally allow two-dimensional (2D) inspections only.

The work herein presented attempts to define a suitable method of evaluating AM multi-material composites. While the approach is flexible for a range of composite structures, consideration of an AM material jetting system is provided. Material jetting systems exploit a piezoelectric ink-jet print head to precisely deposit on demand nano-droplets of photo-curable materials containing a photo initiator. A photo-polymerization system is coupled to the piezoelectric printing head to cure the droplets which then form a solid polymer, layer by layer, onto a building platform known as substrate[10 11]. The light coming from an ultraviolet (UV) lamp activates the curing process of the photopolymer layers, each one sticking to the previous layer until the entire designed part is realised. Typically, these materials are similar in physical characteristics such as density, which makes attempts to differentiate them a challenge using OM and SEM unless variations in surface finish or colour are apparent.

In previous studies[12] optical and SEM investigations were useful to monitor mechanical testing of multi-material composites, which allowed computational predictions on crack development and related energy dissipation/toughening strategies of biologically inspired structures[13 14]. In another study, two materials of contrasting hard and soft mechanical properties were combined to explore the effects of simple 3D chess patterns, printed in a voxel-based manner with varying dimensional parameters to influence the fracture path. SEM was employed to routinely highlight contours of different regions as well as failure lines predominantly propagating through the rigid material during mechanical testing[15].

Despite imaging techniques such as OM and SEM are able to provide topological information on the surface of shaped materials, complementary imaging techniques such as X-ray computed tomography (XCT) are necessary to reveal volumetric information where the other imaging techniques are not practical. Probed samples, whether they are single objects, hierarchical assemblies of materials, exhibit internal features that are detected and reconstructed using computed image techniques based on the interaction of X-rays with matter. Indeed, XCT generates 3-dimensional representations of objects, typically non-destructively, hence allowing sample monitoring before, during and after a particular testing regime is applied to the sample. As composites are used predominantly in structural applications, mechanical testing is usually applied to evaluate deformation and failure of the various constituent materials as well as the resultant structure[16–19] . XCT allows mapping of the effective density distribution in the fabricated part, which predominantly defines the attenuation between the probe X-ray and material. The generated 3D map consists of voxels that are displayed with a greyscale value related to the X-ray attenuation of the material[20 21]. If materials identification is possible, CAD designed features and triangulated surfaces (meshes) resulting from the image processing after XCT scanning can be compared. So far, the use of XCT combined to AM has been primarily oriented to investigate and compare mono-material AM parts against CAD models, thus considering topology primarily. Routine studies have evaluated the porosity of a structure produced from a stereolithography AM process using XCT imaging where the material and porous space provided significant variation in the X-ray probe attenuation with the sample[22]. XCT investigation of AM multi-material structures have been performed to analyse the location, for example, of active pharmaceutical ingredients compacted within a 3D printed carrier[20], evaluate the interfacial density variation between copper and steel and examine alloying of molybdenum particles in titanium parts produced via laser powder bed fusion[23]. In some cases, synchrotron XCT techniques were used to accurately determine distribution of pores and inclusions in the same sample manufactured with laser metal deposition[24].

Currently the use of XCT to determine composition of AM multi-material structures has been neglected especially when employing multi-jetting technology to facilitate the production of polymeric composite structures where different materials within such structures have similar densities[25,26,27]. Understanding the variation in composition for AM multi-material structures has been shown to be important in determining the fracture development of the structure during mechanical loading. Composite materials incorporating bone, biocalcite and bone-like geometries[28,29,30,31] were produced using ink-jetting AM and avoiding multistep parts assembly of soft phase and hard-stiff inclusions to reproduce the mechanical interplay between phases and toughening mechanisms inspired by nature.

In the work presented here, XCT is employed to qualitatively and quantitatively analyse the assembly of ink-jet multi-material AM composites made of soft and hard phases.

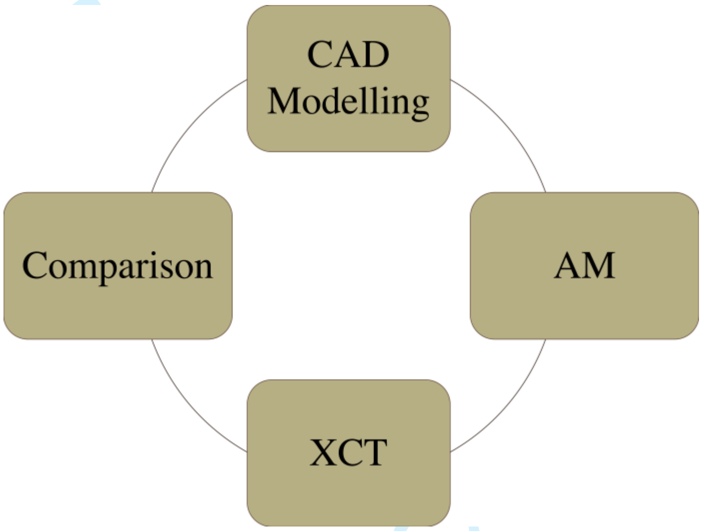

Figure 1. XCT-based workflow to approach and inspect AM composite parts.

A composite structure comprising of a single hard fibre feature embed in a softer matrix material was imaged using XCT. Reconstructed images were analysed in terms of surface area and volume to be compared to the original CAD sources according to the schematic in Figure 1. A critical aim of the evaluations is the potential for XCT to distinguish between different UV curable 3D printing materials but similar in density, hence in X-ray attenuation. Hard and soft materials were allocated to both matrix and inclusion to detect any difference in contrast and shape. The proposed XCT-based workflow aims to compare input drawings with the manufactured ones, maximizing contrast between the fibre and matrix.

Material and Methods

Design and 3D printing

An interlocking single fibre composite was designed in Rhinoceros 3D 5.0 (Robert McNeel and Associates, USA) in the form of complementary regions defined by precise geometrical boundaries. The interlocking shape was chosen to allow warping of thin walls as a result of the manufacturing process, which will then be highlighted within the geometrical difference between the CAD design and the XCT reconstruction. The resultant CAD model is displayed in Figure 2a, where a rectangular feature is included in a matrix characterised by narrow neck (2 mm) and a wide body (10 mm). The nominal thicknesses of the matrix and fibre are 3 mm and 2 mm, respectively. An inkjet-based 3D printer (ProJet 5500X, 3D Systems, USA) allowed for the simultaneous layered deposition of two base materials, namely a hard-white material (VisiJet® CR-WT 200) and a soft black material (VisiJet® CE-BK) from the same 3D printer manufacturer. These materials are referred to in this paper as WT and BK, respectively. The 3D printer resolution was set to an ultra-high definition 13 μm layer thickness (750 x 750 x 2000 Dots per Inch (DPI)), which is the highest performance of the 3D printer used in this study. Two sample configurations of black fibres in a white matrix (BK into WT) and white fibres in a black matrix (WT into BK) were designed (Figure 2b).

XCT evaluation

Evaluations of the 3D printed samples were carried out using an XCT system (Versa 520, Carl Zeiss Microscopy Ltd., USA) operating with a 70 kV/6 W. Polyurethane foam material was used to support and hold in place the parts within a box confining the volume of interest within the XCT system. A 29 μm isotropic voxel size was achieved from imaging samples with a total of 1601 projections over 360°. Each projection was collected at a 2 s exposure time. The reconstruction of image datasets of the two scanned samples was performed using Scout and Scan software (Zeiss) and rendered using XM3DViewer 1.2.8 (Zeiss). Figures 2c and 2d depict the output of the rendering showing the difference between a BK into WT and WT into BK assembly.

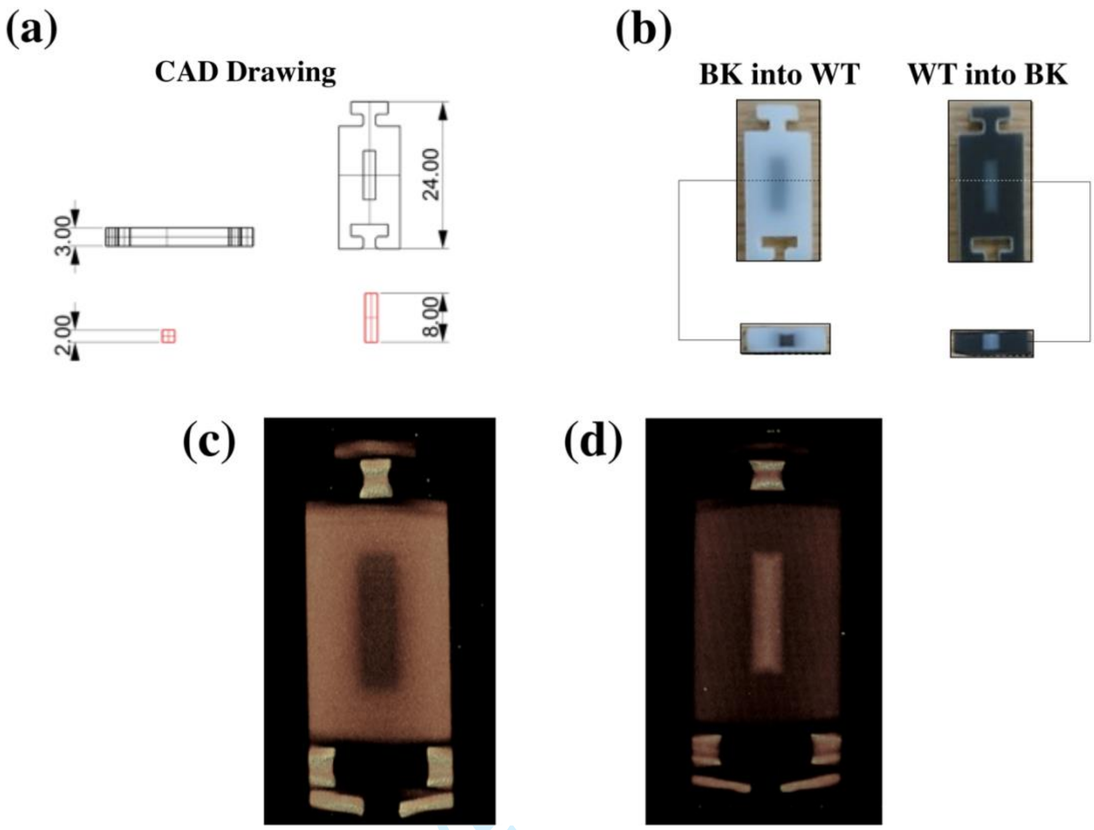

Figure 2. Representation of the interlocking fibre composite. a) CAD drawing of the multi-material part. The matrix is reported in black, the inner fibre in red. All the dimensions are in mm. b) Fabricated parts with complementary materials allocation. XCT reconstruction of the corresponding composites (c) BK in WT and (d) WT in BK.

Image post-processing

The resultant XCT images were post-processed using a semi-commercial software (MeVisLab, MeVis Medical Solutions AG, http://www.mevislab.de/). The post-processing was applied to enhance contrast between the WT and BK materials as well as allowing quantitative comparison between the digital composite designs and the resultant AM physical output. The image processing workflow was built connecting components in a cascade fashion (Figure 3a). X-ray tomograms were imported in MeVisLab to define an interactive reconstruction of Volumes of Interest (VOIs). For the purpose of this study, a visual script aimed at recognising greyscale distribution in the samples was generated and then followed by a procedure of segmentation via region growing to discern different phases. Given the similar densities of the materials used, a filtering procedure based on Gauss smoothing was necessary to homogenise the greyscale value of the voxels belonging to the same phase. The *GaussSmoothing* component provided by MeVisLab, performs an isotropic smoothing to the image dataset in input. A gauss sigma equal to 2 was adopted to set the window of the filter kernel. A calibration step performed on the overall shape of the samples was necessary to verify that the applied Gauss filtering would maintain the same volume of the original geometry. Threshold values to segment VOIs were found analysing the histograms of each data-sets or materials combination. The region growing procedure started with the selection of a *seed* that is a voxel belonging to the considered XCT image dataset. The region was then expanded to neighbouring voxels in which grey values are coincident or fall in an interval defined by the user and named Threshold Interval Size [%]. For this purpose, a seed was placed within the VOI (matrix plus fibre), adopting a threshold interval size to be decreased in a multistep procedure.

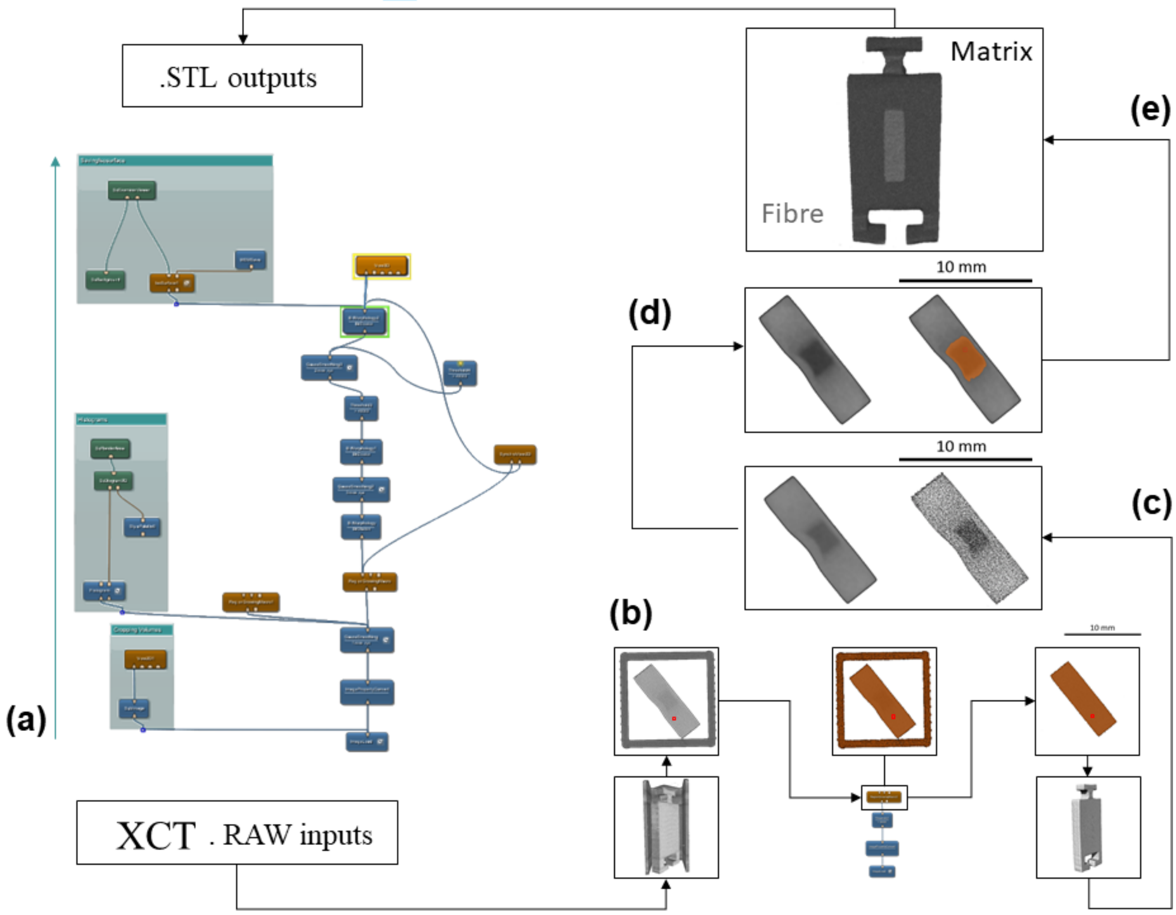

Figure 2. Schematic showing: (a) the overall workflow and the subsequent steps to (b) place the red region growing pixels cluster (seed) into the core region to be separated from the rest; (c) datasets comparison before and after Gauss smoothing to homogenise the highlands effects within the fibre core; (d) region growing procedure starting from the seed previously introduced and (e) the final post-processed imaging highlighting a discrete fibrous object within a matrix.

The multistep procedure aimed to identify the optimum threshold to segment the sample as multi-material piece. Figure 3b describes how to highlight the VOI decreasing the threshold interval size. Once the VOI has been segmented, the second step of the region growing procedure aimed to separate the fibre from the matrix. The two regions are spatially assembled; therefore, the image dataset was processed applying a Gauss smoothing filtering to homogenise pixel intensity (Figure 3c). The contrast between fibre and matrix was enhanced to facilitate a further region growing segmentation, separating fibre from matrix. The fibre itself represents the new VOI; thus, all the grey values belonging to the matrix were neglected. The starting seed was placed in the fibre and multistep procedure used to identify the Threshold Interval Size [%] for both BK fibres into WT matrix and vice versa. The threshold Interval Size [%] in the multistep was decreased to highlight a core volume comparable to the one of the designed fibres.

Meshes geometric difference

Quantification of geometrical differences between CAD and XCT datasets was performed using a Hausdorff distance criterion. Specifically, MeshLab v. 1.3.4beta (Visual Computing Lab, ISTI, CNR) applied a sampling filter called Hausdorff distance, based on the Metro digital tooL[32]. The tool numerically compares two triangulated meshes representing the same surface at different levels of detail. In the current study the two surfaces are represented by the ideal CAD drawing and the resultant reconstructed mesh surface after image processing. The difference between two meshes results in an approximation error that can be defined as the distance between corresponding sections of the meshes. Such differences are evaluated by considering a point p on a surface S, such that a distance to another point can be defined by e (p,S) thus:

$$e\,(p, S) = \min_{p' \in S} d(p, p') \qquad \text{Equation (1)}$$

Where d is the Euclidean distance between two points in the space E_3. The distance between two surfaces S_1 and S_2 is then defined as:

$$E\,(S1, S2) = \max_{p \in s_1} e(p, s_2) \qquad \text{Equation (2)}$$

This definition of distance is not symmetric such as $E(S_1,S_2) \neq E(S_2,S_1)$. A two-sided distance (Hausdorff distance) may be obtained by taking the maximum of $E(S_1,S_2)$ and $E(S_2,S_1)$. The MeshLab command uses a sampling function that computes the aforementioned formula. A number of points p_1 is defined onto a mesh or surface S_1. The search is carried on for each point p_1 to find the closest point p_2 on the mesh or surface S_2. The software reports numerical results in mesh units with a red through green to blue map reporting a corresponding increasing coincidence between the digital design and AM physical object.

Results

Image processing: VOIs thresholding

Figure 4 shows a comparison between the volume segmentation before (RAW dataset) and after the Gauss smoothing.

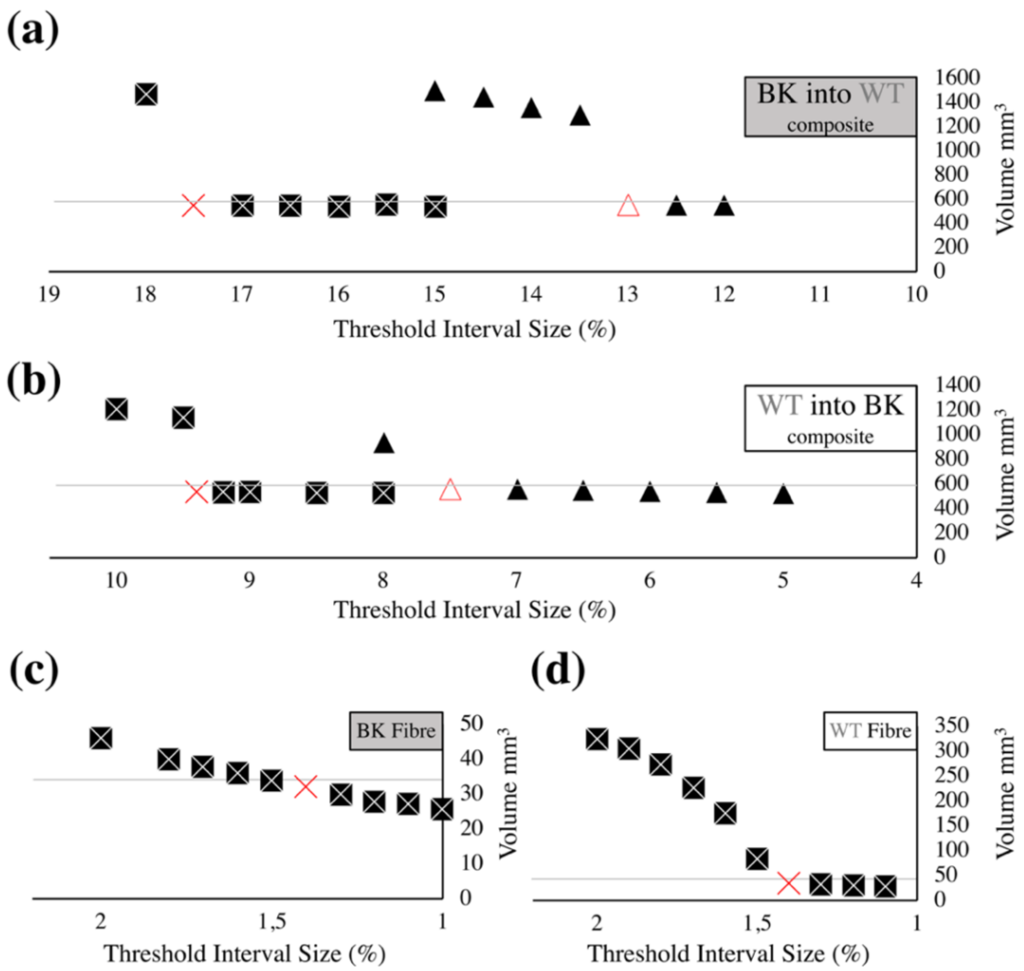

Figure 3. Multistep region growing procedure for (a) BK into WT and (b) WT into BK material composites. The threshold interval size [%] is reported on the x-axis whereas the segmented volume is provided by the

y-axis for each iteration step. The black squares represent for the procedure applied to the. RAW datasets. The triangles draw the trends for the. RAW dataset after Gauss smoothing. The red cross and triangle represent the best threshold interval sizes for each dataset. Finally, the horizontal line traces the best case for the segmentation procedure matching the ideal volume of interest from CAD drawings. Trends for best threshold interval size [%] multistep region growing procedure are depicted for the (c) BK fibre and for the (d) WT fibre.

Threshold interval sizes [%] of 17.5% and 13%, around the volume of the original CAD drawings of 600 mm^3, were identified for BK into WT composite RAW data set and Gauss smoothed (Figure 4a), whereas values of 9.4 % and 7.5 % were found for the WT into BK composite (Figure 4b). Variation in the recorded volume during each iteration of the growth are also shown in Figure 4a for BK into WT and Figure 4b WT into BK. The original CAD drawing defined a target fibre volume of 32 mm^3, which was reached in Figure 4c and Figure 4d for optimised threshold interval sizes of 1.2% and 1.4%.

Table 1. Geometrical dimensions from CAD drawings compared to those of the reconstructed meshes after XCT scanning of BK into WT and WT into BK materials. Absolute relative changes are reported as percentage of the CAD values.

Triangulates surfaces comparison

	CAD	BK into WT	WT into BK	Abs. Relative Difference (%)	
				BK into WT	WT into BK
Matrix Volume (mm^3)	600.0	554.2	542.9	7.6	9.5
Fibre Volume (mm^3)	32.0	31.4	30.8	1.9	3.7
Matrix Surf. Area (mm^2)	669.8	635.6	637.2	5.1	4.9
Fibre Surf. Area (mm^2)	72.0	71.2	70.8	1.1	1.7
Matrix width (mm)	10.0	9.9	10.1	1.5	1.1
Fibre width (mm)	2.0	2.6	2.3	30.0	15.0
Matrix length (mm)	24.0	23.9	24.0	0.4	0.2
Fibre lenght (mm)	8.0	8.6	8.1	7.5	1.2
Matrix thickness (mm)	3.0	3.2	3.2	6.6	6.7
Fibre thickness (mm)	2.0	1.9	2.2	5.0	10.0

A further investigation was carried out in CAD environment to provide insights into the accuracy of the reconstructed VOIs in terms of linear measurements of width, length and thickness. Table 1 outlines the results of several geometrical comparisons referring to reconstructed meshes to the original CAD drawing. The analysed parameters were volume, surface area, width, length and thickness for both the reconstructed fibre and matrix. To have comparable measurements, geometries were aligned in x, y and z axis and bounding box volumes retrieved. For consistency, the fibre and matrix lengths, widths and thicknesses measurements were taken from the bounding box. Surface area and volume were evaluated again in the 3D modelling environment Rhinoceros.

Meshes geometrical differences

Resultant Hausdorff distance maps are shown in Figure 5. Red and blue are the boundary colours representing distances between the meshes (0.00 mm to 0.38 mm) for the matrix and (0.00 mm to 0.49 mm) for the fibre, respectively. The BK fibre into the WT matrix displayed maximum Hausdorff distances of 0.38 mm (Figure 5a) and 0.49 mm (Figure 5 a1) for the matrix and fibre respectively, whereas the WT into BK composite showed smaller distances for matrix (0.38 mm, Figure. 5b) and fibre (0.38 mm, Figure 5 b1).

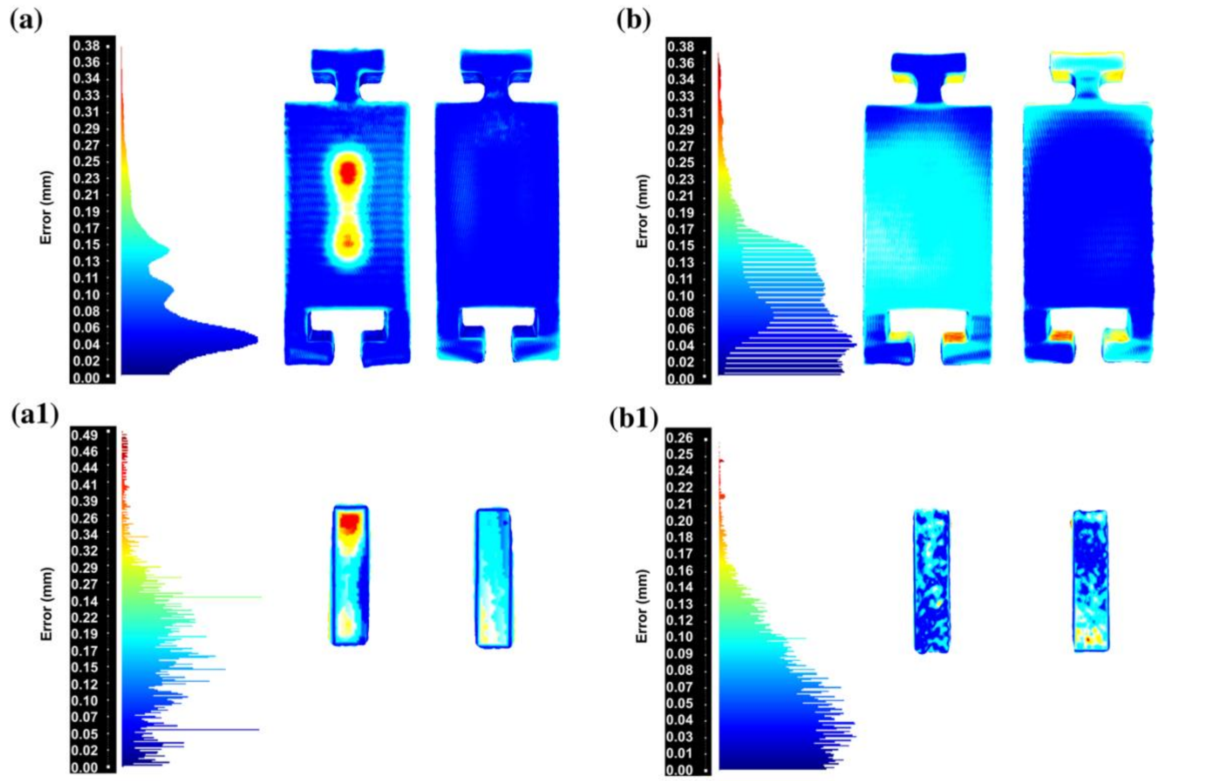

Figure 5. Geometrical difference applied to the reconstructed VOIs using the Hausdorff distance in Meshlab for matrix (top) and fibre (bottom). The reconstructed geometries were compared with the respective CAD drawings, BK into WT (a, a1) and WT into BK (b, b1). The distance range is visually reported and represented by a shade of colours that goes from blue to red accompanied by the relative variation.

Discussion

Multi-material AM avoids multistep parts assembly typical of composites materials manufacturing. A full exploitation of multi-material AM requires a complete examination of the 3D printed builds for modelling purposes and to eventually rely on composite theories for prediction and tuning of the mechanical interplay between composite phases. Although 3D printing can accurately reproduce specific designed models, the prints can deviate from the designed models. For this reason, volumetric information is needed and XCT is clearly advantageous when compared to other imaging techniques that are constrained to 2D investigation. XCT systems have been designed for applications of industrial metrology becoming the only commercially-available, non-destructive method to perform dimensional measurements of internal geometrical features[33 34]. Among all the added benefits of a non-destructive volumetric investigation, XCT 3D representations of objects can be processed and analyzed to be further compared to their original drawings, showing coincidence between manufactured and digital volumes. So far, XCT has been mainly employed to determine distribution of random inclusion in the same manufactured sample, evaluate distribution of pores, interfacial density variation between different phases as well as degradation of pharmaceutical 3D printed drug delivery dosage forms[22 20 23 24]. Although material extrusion such as FDM is commonly used in prototyping composite parts, AM technologies such as ink-jet printing, are now capable of producing higher resolution parts with improved densities and mechanical properties[33]. Particularly, ink-jetting gained attention as a credible industrial method, due to its scalability and multi-material part production[35] and a better understanding of geometrical variations in the 3D printed build relative to the different materials used to produce the multi-material composite is of paramount importance.

The aim of this study is to implement a procedure able to qualitatively and quantitatively analyse the direct assembly of ink-jet 3D printed composites. The proposed workflow was able to determine the composition of a single fibre composite that is a simplified version of AM polymeric composites previously proposed [25 26 27]. Differentiating the core fibre from the bulk within AM composite with XCT resulted challenging mostly due to the presence of phases with similar densities. Most ink-jet print heads work best with inks of low viscosity at/or near room temperature[33]. This could be impairing XCT ability to discriminate elements with similar attenuation and dimensions, such as ink-jets. To be effective XCT needs to be coupled with imaging techniques able to reconstruct and partition regions in an image. To this purpose Gaussian smoothing was used to `blur' images and remove detail and noise. In this sense it is similar to the mean filter but it uses a different kernel that represents the shape of a Gaussian (`bell-shaped') hump. One of the principal reasons for using a Gauss filter is due to its frequency response able to reduce the high spatial frequency components from an image[36]. Compared to other linear filters such as the Mean filter, gaussian blurring is a linear operator rather than non-linear. Contrary to the mean filters which performs a uniform weighted average, the degree of smoothing of a gaussian filter is determined by the gaussian standard deviation; the output represents a weighted average of each voxel's neighborhood rather than uniform smoothing. Other filters such as the Median are non-linear and are famous to remove details and noise and to preserve edges[37]. In the case of this study edges were reconstructed combining the Gaussian operator to a region growing procedure due to the fact that edges where not defined. Indeed, what appeared as a cluster of islands in the data sets core region, were joined to form a boundary that reflected the fibre shape. This aspect was fundamental for the XCT visualisation of the fibre core region in this study. Moreover, a complementary materials allocation WT into BK and WT into BK was considered to understand how this could affect the manufacturing process hence deviating from the original CAD design according to different materials allocation. The gauss filter successfully smoothed and interconnect the sub-regions in the fibres, enhancing the contrast between matrix and fibre. Finally, a multistep region growing procedure helped in defining thresholding values to isolate a continuous fibre from the external matrix.

Further analysis in terms of surface area and volume were performed on the resulting meshes STL and directly compared to files CAD source after both XCT datasets were converted into STL files to perform a geometrical difference with the CAD drawing. Table 1 allows critical considerations of the investigated material assemblies. The volume of the whole sample was coincident to the CAD model in terms of volume and surface area where the largest discrepancy was shown from the BK fibre into the WT matrix. A decrease in volume for both samples BK into WT and WT into BK of 7.6% and 9.5 % respectively, can be related to either the XCT voxel size or material behaviour during production. The volume of the embedded fibres was almost replicated with the digital design, showing a 3.7% and 1.9% volume reduction in comparison to the original CAD drawing of the fibre. The surface area of the matrix and fibre for both material combinations slightly differed from the design, showing a maximum of 5.1% surface area loss for BK into WT composite. Width, length and thickness of the parts and the fibre all differed for less than a 10% compared to the CAD drawing, except for the widths of the fibre, which were found to be bigger by 30% and 15% for the BK into WT and WT into BK, respectively. This can be explained by referring to the ink-jet AM process, which uses a roller/planerizer in order to flatten the printed parts and remove bubbles and excess of material from the printed layer, according to the resolution set for the AM process[38]. Critically, the fibre core of the composite, is still partially cured by the UV light when the roller passes onto the layer, spreading the core in the XY plane while pushing the fibre to spread at the interface into the matrix. This appears to be more effective for the combination BK into WT where the black elastomeric material is the fibre.

Conclusion

An original metrology tool applied to multi-material AM composites has been investigated within this study. Two different allocation of materials, BK into WT and WT into BK, were considered to investigate manufacturing fidelity when fibre and matrix were mutually produced with rigid WT and flexible BK materials, but complying with the same CAD drawing. XCT helped to produce a virtual model of the 3D printed part, showing regions very similar in density, hence difficult to be distinguished and compared. In order to stabilize the workflow, the procedure considered a region growing calibration step performed on the overall shape of the samples without considering the embedded fibre. This study demonstrates the viability of XCT to quantitatively analyse AM multi-materials prototypes made of soft and hard phases produced via ink-jet AM. This investigation was relevant in defining design boundary conditions below which features are partially reproduced in respect to the original digital drawings, with the potential of affecting the phases mechanically interplay, which is fundamental for materials science and engineering composite applications.

Acknowledgements

Marco Curto was funded by a University of Portsmouth (UoP) PhD Scholarship award. All authors acknowledge the Zeiss Global Centre and Future Technology Centre (FTC) at UoP for providing imaging and manufacturing facilities.

References

1. Le, V., Paris, H. & Mandil, G. Using additive and subtractive manufacturing technologies in a new remanufacturing strategy to produce new parts from End-of-Life parts Abstract : *22 ème Congrès Français Mécanique CFM2015* 1–8 (2015). doi:10.13140/RG.2.1.2442.3129

2. Barthelat, F. Nacre from mollusk shells: A model for high-performance structural materials. *Bioinspiration and Biomimetics* **5**, 1–8 (2010).

3. X. Gu, G. *et al.* Three-Dimensional-Printing of Bio-Inspired Composites. *J. Biomech. Eng.* **138**, 021006 (2016).

4. ASTM International. F2792-12a - Standard Terminology for Additive Manufacturing Technologies. *Rapid Manuf. Assoc.* 10–12 (2013). doi:10.1520/F2792-12A.2

5. Yang, S. & Zhao, Y. F. Additive manufacturing-enabled design theory and methodology: a critical review. *Int. J. Adv. Manuf. Technol.* **80**, 327–342 (2015).

6. Yang, H. *et al.* Performance evaluation of ProJet multi-material jetting 3D printer. *Virtual Phys. Prototyp.* **12**, 95–103 (2017).

7. Hull, C. W. & Arcadia, C. Us4575330a. (1984). doi:US005485919A

8. Singh, M., Haverinen, H. M., Dhagat, P. & Jabbour, G. E. Inkjet printing-process and its applications. *Adv. Mater.* **22**, 673–685 (2010).

9. Fantini, M. & Curto, M. Interactive design and manufacturing of a Voronoi-based biomimetic bone scaffold for morphological characterization. *Int. J. Interact. Des. Manuf.* 1–12 (2017). doi:10.1007/s12008-017-0416-x

10. Smith, P. J. & Morrin, A. Reactive inkjet printing. *J. Mater. Chem.* **22**, 10965–10970 (2012).

11. Wang, T., Patel, R. & Derby, B. Manufacture of 3-dimensional objects by reactive inkjet printing. *Soft Matter* **4**, 2513–2518 (2008).

12. Dimas, L. S. & Buehler, M. J. Modeling and additive manufacturing of bio-inspired composites with tunable fracture mechanical properties. *Soft Matter* **10**, 4436–4442 (2014).

13. de Obaldia, E. E., Jeong, C., Grunenfelder, L. K., Kisailus, D. & Zavattieri, P. *Analysis of the mechanical response of biomimetic materials with highly oriented microstructures through 3D printing, mechanical testing and modeling*. *Journal of the Mechanical Behavior of Biomedical Materials* **48**, (2015).

14. Feilden, E. *et al.* 3D Printing Bioinspired Ceramic Composites. *Sci. Rep.* **7**, 1–9 (2017).

15. Swetly, T. *et al.* Bioinspired engineering polymers by voxel-based 3D-printing. *BioNanoMaterials* **17**, 145–157 (2016).

16. Soutis, C. Fibre reinforced composites in aircraft construction. *Prog. Aerosp. Sci.* **41**, 143–151 (2005).

17. Naslain, R. R. SiC-matrix composites: Nonbrittle ceramics for thermo-structural application. *Int. J. Appl. Ceram. Technol.* **2**, 75–84 (2005).

18. Hufenbach, W. *et al.* Polypropylene/glass fibre 3D-textile reinforced composites for automotive applications. *Mater. Des.* **32**, 1468–1476 (2011).

19. Esser-Kahn, A. P. *et al.* Three-dimensional microvascular fiber-reinforced composites. *Adv. Mater.* **23**, 3654–3658 (2011).

20. Markl, D. *et al.* Analysis of 3D Prints by X-ray Computed Microtomography and Terahertz Pulsed Imaging. *Pharm. Res.* **34**, 1037–1052 (2017).

21. du Plessis, A., Yadroitsev, I., Yadroitsava, I. & Le Roux, S. G. X-Ray Microcomputed Tomography in Additive Manufacturing: A Review of the Current Technology and Applications. *3D Print. Addit. Manuf.* **5**, 3dp.2018.0060 (2018).

22. Melchels, F. P. W. *et al.* Mathematically defined tissue engineering scaffold architectures prepared by stereolithography. *Biomaterials* **31**, 6909–6916 (2010).

23. du Plessis, A., Yadroitsev, I., Yadroitsava, I. & Le Roux, S. G. X-Ray Microcomputed Tomography in Additive Manufacturing: A Review of the Current Technology and Applications. *3D Print. Addit. Manuf.* **5**, 227–247 (2018).

24. Xavier, M. S. *et al.* Nondestructive quantitative characterisation of material phases in metal additive manufacturing using multi-energy synchrotron X-rays microtomography. *Int. J. Adv. Manuf. Technol.* **106**, 1601–1615 (2020).

25. Parwani, R. *et al.* Morphological and Mechanical Biomimetic Bone Structures. *ACS Biomater. Sci. Eng.* **3**, 2761–2767 (2017).

26. Compton, B. G. & Lewis, J. A. 3D-printing of lightweight cellular composites. *Adv. Mater.* **26**, 5930–5935 (2014).

27. Ebert, L. C., Thali, M. J. & Ross, S. Getting in touch-3D printing in Forensic Imaging. *Forensic Sci. Int.* **211**, 1–6 (2011).

28. McGurk, M., Amis, A. A., Potamianos, P. & Goodger, N. M. Rapid prototyping techniques for anatomical modelling in medicine. *Ann. R. Coll. Surg. Engl.* **79**, 169–174 (1997).

29. Dimas, L. S., Bratzel, G. H., Eylon, I. & Buehler, M. J. Tough composites inspired by mineralized natural materials: Computation, 3D printing, and testing. *Adv. Funct. Mater.* **23**, 4629–4638 (2013).

30. Mitchell, M. J. & King, M. R. NIH Public Access. 1–23 (2014). doi:10.1088/1367-2630/15/1/015008.Fluid

31. Mirzaali, M. J. *et al.* Mechanics of bioinspired functionally graded soft-hard composites made by multi-material 3D printing. *Compos. Struct.* **237**, (2020).

32. Cignoni, P., Rocchini, C. & Scopigno, R. Metro: Measuring Error on Simplified Surfaces. *Comput. Graph. Forum* **17**, 167–174 (1998).

33. Rashid, A. *Additive Manufacturing Technologies*. *CIRP Encyclopedia of Production Engineering* (2019). doi:10.1007/978-3-662-53120-4_16866

34. Villarraga, H., Morse, E., Hocken, R. & Smith, S. Dimensional metrology of internal features with X-ray computed tomography. *Proc. - ASPE 2014 Annu. Meet.* 684–689 (2014).

35. Wijshoff, H. The dynamics of the piezo inkjet printhead operation. *Phys. Rep.* **491**, 77–177 (2010).

36. R., A. & L., A. A Review on Image Enhancement Methods. *Int. J. Comput. Appl.* **164**, 4–9 (2017).

37. Kowalski, P. & Smyk, R. Review and comparison of smoothing algorithms for one-dimensional data noise reduction. *2018 Int. Interdiscip. PhD Work. IIPhDW 2018* 277–281 (2018). doi:10.1109/IIPHDW.2018.8388373

38. Yang, H. *et al.* Performance evaluation of ProJet multi-material jetting 3D printer. *Virtual Phys. Prototyp.* **12**, 95–103 (2017).